$YCa_3(CrO)_3(BO_3)_4$: a new Cr^{3+} kagomé lattice compound

Chun-Hai Wang[1], *Maxim Avdeev*[2], *Brendan J. Kennedy*[1], *Michael Küpers*[3], *and Chris D. Ling*[1,*]

[1]School of Chemistry, the University of Sydney, Sydney 2006, Australia.

[2]Bragg Institute, Australian Nuclear Science and Technology Organisation, Menai 2234, Australia.

[3]Institute of Inorganic Chemistry, RWTH Aachen University, 52056 Aachen, Germany

ABSTRACT: We report a new gaudefroyite-type compound $YCa_3(CrO)_3(BO_3)_4$, in which Cr^{3+} ions ($3d^3$, S = 3/2) form an undistorted kagomé lattice. Using a flux agent, the synthesis was significantly accelerated with the typical calcining time reduced from more than two weeks to two days. The structure of $YCa_3(CrO)_3(BO_3)_4$ was determined by combined Rietveld refinements against X-ray and neutron diffraction data. Symmetry distortion refinement starting from a disordered $YCa_3(MnO)_3(BO_3)_4$ model was applied to avoid over-parameterization. There are two ordering models, K2-1 and K2-2 with the space groups $P6_3$ (#173) and $P\bar{3}$ (#147) respectively that differ in the $[BO_3]$ ordering between different channels (in-phase or out-of-phase). Both models give similarly good fits to the diffraction data. $YCa_3(CrO)_3(BO_3)_4$ is an insulator with the major band gap at E_g = 1.65eV and a second transition at 1.78 eV. Magnetically, $YCa_3(CrO)_3(BO_3)_4$ is dominated by antiferromagnetic exchange along edge-sharing CrO_6 octahedral chains perpendicular to the kagomé planes, with $\Theta \approx -120$ K and $\mu_{eff} \approx 3.92\ \mu_B$. The compound shows no spin ordering or freezing observed down to at least 2 K.

KEYWORDS: kagomé lattice, geometrically frustrated magnetism, transition metal borate, chromium (III) oxide

INTRODUCTION

Frustrated antiferromagnetic systems continue to attract considerable interest as these systems have a large ground state degeneracy, making them an interesting platform for theoretical and experimental physicists to explore the possible ground states and their entanglements[1-4]. Geometrically frustrated magnetism (GFM) occurs in systems where magnetic cations (spins) are located on a lattice with a triangular geometry and there are antiferromagnetic interactions among them, such that the three neighbouring spins on a triangle cannot be simultaneously antiparallel to each other. There are several ideal GFM lattice motifs, notably the 2D triangular, 2D kagomé, and 3D pyrochlore lattices. In an ideal GFM system, spin liquid (e.g., $Tb_2Ti_2O_7$[5]) or spin ice (e.g., $Ho_2Ti_2O_7$[6]) behaviour is expected. However, in some cases spin glass behaviour is observed due to the freezing of the spins upon cooling. One such case is the mineral gaudefroyite $Ca_4(MnO)_3(BO_3)_3CO_3$, a rare example of a physical realization of the kagomé lattice in a natural mineral. It was first identified in minerals from the Tashgagalt mine in Morocco by Jouravsky and Permingeat[7] and its structure determined by Granger and Protas[8] as consisting of 2D layers of MnO_6 octahedra with Mn^{3+} cations arranged in a perfect kagomé lattice, connected by trigonal CO_3^{2-} units. The Ca^{2+} ions are ordered in the hexagonal channels perpendicular to the layer stacking axis. Edge-sharing MnO_6 octahedra form continuous chains perpendicular to the kagomé planes. At high temperatures the magnetic behavior of $Ca_4(MnO)_3(BO_3)_3CO_3$ is dominated by ferromagnetic (FM) exchange along these chains, and it undergoes a spin-glass freezing transition on cooling below $T_f = 10$ K[9].

The synthetic compounds $YCa_3(MO)_3(BO_3)_4$ (M is a trivalent cation) are structurally related to gaudefroyite, formed by substituting BO_3^{3-} for CO_3^{2-}, as well as Y^{3+} for a Ca^{2+} site to maintain

charge neutrality. Four $YCa_3(MO)_3(BO_3)_4$ compounds have been reported to date with M = Al, Ga, Mn, and V [10-12]. Considering the magnetic cation, Mn^{3+} (high-spin $3d^4$, $S = 2$) and V^{3+} ($3d^2$, $S = 1$), both $YCa_3(MnO)_3(BO_3)_4$ and $YCa_3(VO)_3(BO_3)_4$ are expected to be GFM systems. Li and Greaves[11] first studied the structure and magnetic properties of $YCa_3(MnO)_3(BO_3)_4$. They described the structure of $YCa_3(MnO)_3(BO_3)_4$ using a hexagonal $P6_3/m$ (Space Group 176) unit cell and observed ferromagnetic (FM) behaviour within the Mn chains and antiferromagnetic (AFM) ordering in the kagomé plane at 7.5 K. The structure of $YCa_3(MnO)_3(BO_3)_4$ is shown in Figure 1. The [MnO_6] octahedra are connected by [BO_3] groups to form a kagomé lattice in the *a–b* plane. The kagomé planes are further connected *via* edge-sharing [MnO_6] octahedra and [BO_3] groups along the *c* axis to form hexagonal and trigonal channels (Figure 1c,d). The hexagonal channels (ch-H) are filled by Y/Ca and [BO_3] groups, whist the smaller trigonal channels (ch-T) are filled by Y/Ca only. Thus there are two different types of [BO_3] groups: framework and channel [BO_3]. The channel [BO_3] groups randomly sit on the two different possible sites in the channel. We subsequently synthesised and investigated $YCa_3(VO)_3(BO_3)_4$ and found that its structure should be described in a tripled unit cell, relative to that of $YCa_3(MnO)_3(BO_3)_4$ (transformation matrix: [(2,1,0)(-1,1,0)(0,0,1)]), in which half of the ch-H channels have ordered [BO_3] groups [12]. The space group of $YCa_3(VO)_3(BO_3)_4$ is $P\bar{3}$ (147). Magnetic property measurements showed that $YCa_3(VO)_3(BO_3)_4$ is a highly frustrated GFM system, with no spin ordering or spin freezing observed down to 2 K.

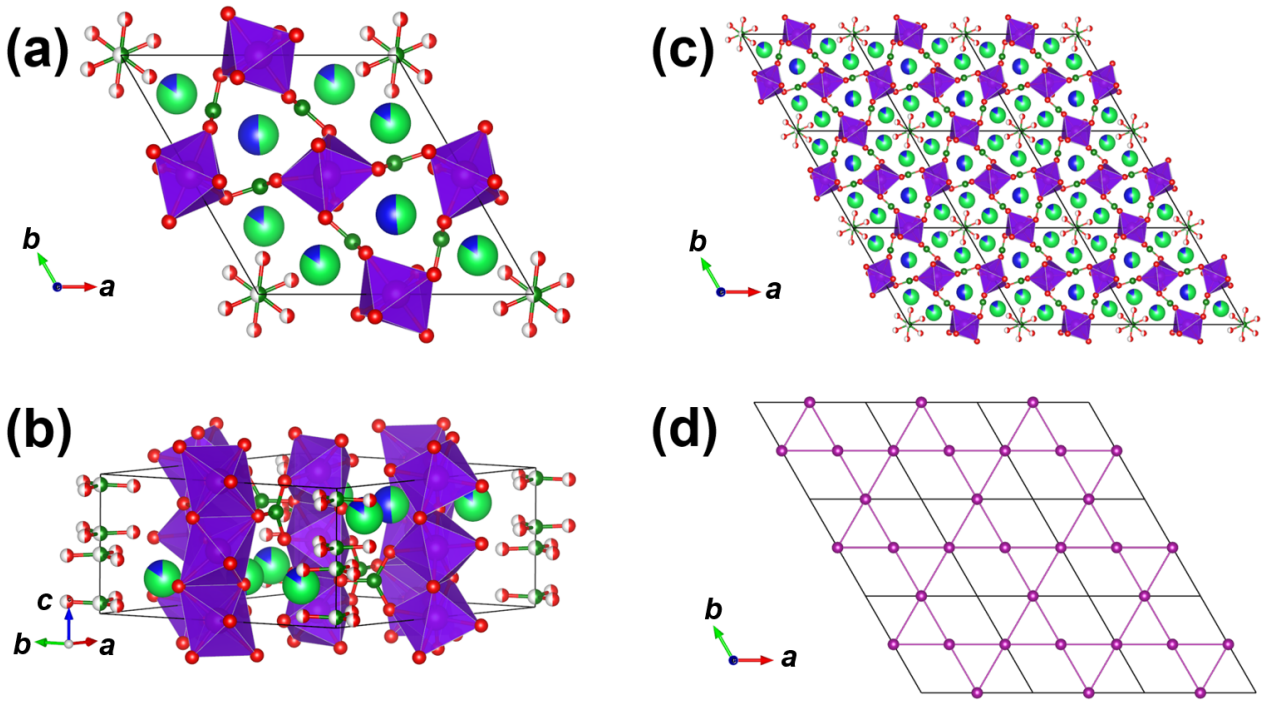

Figure 1. The structure of $YCa_3(MnO)_3(BO_3)_4$.[11] (a) top view along c axis; (b) side view; (c) top view of a 3a × 3b unit cell; (d) Mn^{3+} kagomé lattice. Red = O, small green = B, blue = Y, big green = Ca. [MnO_6] octahedra are drawn. The partial colouring of balls indicates mixed occupancy.

The present work reports the first synthesis and characterisation of $YCa_3(CrO)_3(BO_3)_4$. Strong magnetic frustration of Cr^{3+} ($3d^3$) cations with a kagomé geometry has been observed in several systems[13-15], therefore, $YCa_3(CrO)_3(BO_3)_4$ is also expected to be a strong GFM system. The synthesis of $YCa_3(MO)_3(BO_3)_4$ (M = Al, Ga, Mn, V) from solid state reaction method is very slow and generally requires several weeks at ~1000 °C[10-12] (noting that it is infeasible to calcine at a higher temperature because borate systems are easily vitrified). Consequently we developed a flux synthesis method for $YCa_3(CrO)_3(BO_3)_4$, which significantly accelerated the reaction and allowed us to prepare this new phase.

EXPERIMENT SECTION

Polycrystalline $YCa_3(CrO)_3(BO_3)_4$ was synthesized by solid-state reaction. Stoichiometric amounts (total 3g) of Y_2O_3 (99.99%, Aldrich, heated at 1000 °C before use), $CaCO_3$ (99.99%, Aldrich, heated at 400 °C before use), Cr_2O_3 (99.999%, Aithaca), H_3BO_3 (99.5%, Vnicar) and 0.5g KCl (99.5%, Merck, used as flux) were weighed and ground in an agate mortar and pestle. The well-mixed powders were placed into an open alumina crucible and calcined at 1000 °C (ramp at 5°C /min) for 24 h. After cooling, the samples were ground and reheated at 1000 °C for 48 h (heating the sample at temperatures higher than 1100 °C caused the sample to melt and vitrify). After the reaction, dark green $YCa_3(CrO)_3(BO_3)_4$ was obtained with the purity ≥ 95%. The impurities were identified as $Ca_2B_2O_5$ and YBO_3. No KCl was observed from the diffraction measurement, indicating that the KCl acted as flux and evaporated during the reaction.

Powder X-ray diffraction (XRD) data of $YCa_3(CrO)_3(BO_3)_4$ were collected at room temperature using a PANalytical X'Pert diffractometer. The data were collected from 5–130° 2θ in reflection mode with a maximum intensity count of ~40 000 under Cu Kα radiation (tube conditions: 40 kV, 40 mA).

Powder neutron diffraction (ND) data were collected on the high-resolution powder diffractometer Echidna at the OPAL research reactor, ANSTO, Australia[16]. A ~2 g polycrystalline sample was loaded in a 6 mm diameter vanadium can and ND data were collected at room temperature, using neutrons of wavelength $\lambda = 2.4395$ Å.

The structure of $YCa_3(CrO)_3(BO_3)_4$ was investigated by combined Rietveld refinements against XRD and ND data, providing the best possible resolution of all the elements by exploiting their different relative X-ray and neutron scattering factors. TOPAS Academic (TA)[17,18] was employed during the Rietveld refinements and an intensity weighting (5%) was applied to the XRD data to

keep a reasonable weighting for both the XRD and ND data during the refinement. Meanwhile, a cylindrical absorption [refined $\mu r \sim 1.9(1)$] was applied to the neutron data due to the neutron absorption of B atoms. For the refinements, three steps were applied to avoid possible over-parameterization and to keep the refinement reliable. Step 1 was to build and refine (Ca/Y occupancy and all free coordinates) a structural model based on that of $YCa_3(MnO)_3(BO_3)_4$. The occupancy of channel [BO_3] units was fixed to 0.5 by the site multiplicity of the space group. The refined model is labelled as Model I. Step 2 used symmetry representation analysis in ISODISTORT[19], according to the observed supercell reflections, to build and refine an ordered cell, Model II, starting from Model I. During this refinement the displacement symmetry modes and channel [BO_3] occupancy modes were refined and screened. In this step, a statistically reliable and chemically reasonable refinement result was achieved. In Step 3 we allowed all free atomic coordinate parameters and the Y/Ca and channel [BO_3] occupancies of Model II to refine, leading to the final structure model (Model III). Note that during this refinement, loose bond length restraints were applied to the B-O bonds (1.37±0.02 Å, with the same weighting to all other parameters).

DC magnetic susceptibility and magnetization data for $YCa_3(CrO)_3(BO_3)_4$ were collected on a Quantum Design Physical Property Measurement System (PPMS) using the vibrating sample magnetometer (VSM) method. Temperature-dependent susceptibility data were collected under zero field-cooled (ZFC) and field-cooled (FC) conditions in a coercive field of 1000 Oe between 2 and 300 K. Additional susceptibility data were collected in coercive fields of 0.5, 1 and 5 T. Field-dependent magnetisation measurement were carried out at 2, 6, 10 and 20 K up to 9 T. Molar magnetic parameters were calculated with respect to the magnetic Cr^{3+} ions [per Cr^{3+}, *i.e.*, 1/3 of a

formula unit $YCa_3(CrO)_3(BO_3)_4$]. Specific heat measurements were carried on the same platform over the temperature range 1.9–150 K.

The conductivity of a $YCa_3(CrO)_3(BO_3)_4$ pellet was recorded using a MTZ-35 impedance analyzer (Bio-Logic) from RT to 700°C. The ac (1V) sweeping range was selected as $0.1 - 1 \times 10^7$ Hz.

Absorption/reflection spectra of $YCa_3(CrO)_3(BO_3)_4$ was measured using a UV-Vis-NIR spectrophotometer (CARY5000, Agilent Technologies) with a Harrick Praying Mantis solid-state reflection accessory. Dried and well-ground NaCl powder was used as reference, the band gap of which (E_g) is 8.5 eV[20]. The wavelength scanning mode was used for data collection.

RESULTS AND DISCUSSIONS

Structure of $YCa_3(CrO)_3(BO_3)_4$. The majority of the peaks in the XRD and ND patterns of $YCa_3(CrO)_3(BO_3)_4$ could be indexed to the $YCa_3(MnO)_3(BO_3)_4$ $P6_3/m$ (S.G. 176) model (Model I). Rietveld refinement of this model yielded fit statistics R_{wp} (overall) = 4.15%, R_{wp} (XRD) = 2.90%, and R_{wp} (ND) = 5.71%. The refined site occupancies were Ca/Y = 0.255/0.745(8) at the 2*c* site and 0.915/0.085(3) at the 6*h* site. This is a higher degree of Ca/Y ordering than reported for $YCa_3(MnO)_3(BO_3)_4$ [Ca/Y = 0.49/0.51(2) at the 2*c* site and 0.837/0.163(3) at the 6*h* site][11]. The refined XRD and ND profiles using Model I are shown in Figure S1 in the Supporting Information (SI) file. This model could not, however account for two obvious peaks (Figure 2a) in the ND pattern, at $2\theta \approx 50.14°$ (d = 2.88 Å) and 55.44° (d = 2.62 Å). These peaks are very weak (~ 3% of the highest peak) in the XRD patterns and are due to ordering of the $[BO_3]$ groups, whose X-ray scattering factor (proportion to the atomic number) is much smaller than that of the heavy atoms. The neutron scattering lengths of the atoms in $YCa_3(CrO)_3(BO_3)_4$ [B: 5.30(4) fm, O: 5.803(4) fm,

Ca: 4.70(2) fm, Cr: 3.635(7) fm, and Y: 7.75(2) fm[21]] are all comparable. Consequently, the reflections from ordering of the [BO_3] groups have appreciable intensity in the ND data. These two peaks, as well as the remainder of the pattern, could be indexed using a tripled unit cell (supercell) with the cell transformation matrix [(2,1,0)(-1,1,0)(0,0,1)], which is the same unit cell as identified by Miiller *et al*. for $YCa_3(VO)_3(BO_3)_4$[12]. Thus, the structure of $YCa_3(CrO)_3(BO_3)_4$ can be considered as a distortion of Model I at the **K** (1/3, 1/3, 0) point[19]. There are four possible **K** distortion irreducible representations (IR): K1, K2, K3K5, and K4K6. All the possible representations were tested and K2 was found to yield the best fit to the $2\theta \approx 50.14°$ and 55.44° ND peaks. There are then two ordering models, K2-1 and K2-2, depending on the ordering relationship between different channels, having space group $P6_3$ (#173) and $P\bar{3}$ (#147) respectively. The XRD and ND data were both well described by adding six displacement mode parameters and four occupancy mode parameters to Model I. Both models yielded good fits to the XRD and ND data after Rietveld refinement (Step 3) with similar overall R_{wp} factors. The Rietveld refinement profiles of XRD and ND data over selected 2θ ranges (5-40° for XRD and 10-60° for ND) for Models I, K2-1 and K2-2 are shown in Figure 2 (all refined profiles are in Figure S1 in the SI file). Crystallographic information files (CIFs) for Models I, K2-1 and K2-2 are available in the SI files. The final fit parameters were R_{wp} (overall) = 3.78%, R_{wp} (XRD) = 2.78%, R_{wp} (ND) = 5.08% for Model K2-1 and R_{wp} (overall) = 3.82%, R_{wp} (XRD) = 2.76%, and R_{wp} (ND) = 5.18% for Model K2-2. The refined cell parameters of these two models are listed in Table 1 and Table 2.

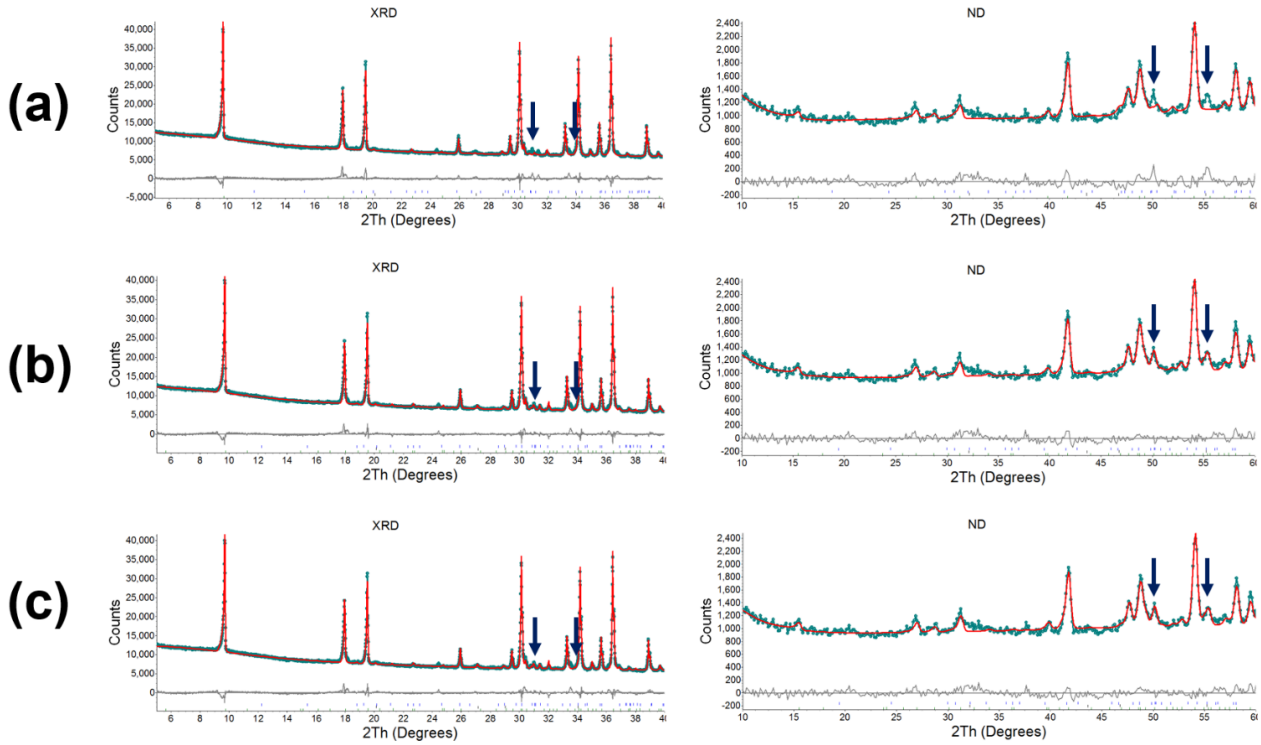

Figure 2. Rietveld refinement profiles of $YCa_3(CrO)_3(BO_3)_4$ at selected 2θ range using three models (a) Model I, (b) Model K2-1 and (c) Model K2-2. Left: XRD; right: ND; Dots, observed; solid line, calculated curve; gray line below, difference curve; vertical tick marks, peak positions. The arrows indicate the positions of the ordering reflections.

It should be noted that Models K2-1 and K2-2 are mathematically different: e.g., there is reflection condition $l = 2n$ for the (000l) reflections in space group $P6_3$; while there is no reflection conditions for space group $P\bar{3}$. The theoretical relative intensity of the (0001) peak in Model K2-2 is ~0.9 % for ND and ~0.5% for XRD, which is too weak to be clearly observed in our data. In addition, the theoretical relative intensity of corresponding reflections is less than 4% in XRD and ND, which again could not be distinguished from the XRD and ND data. However, the Model K2-1 ($P6_3$) is non-centrosymmetric and enantiomorphic whist the K2-2 ($P\bar{3}$) is centrosymmetric. Thus, these two models can be distinguished by symmetry-related property measurements, such

as second-harmonic generation effect (SHG)[22]. Note that the reported structure of $YCa_3(VO)_3(BO_3)_4$[12] corresponds to our K2-2 model.

The structures of Models K2-1 and K2-1 are shown in Figure 3. In some of the Hex-channels, the [BO_3] units are completely ordered with the refined occupancies >0.99. However, in the other Hex-channels the [BO_3] moieties are partially ordered, e.g., 0.80:0.20:1.00:0.00 in Model K2-1 and 0.65:0.35:0.35:0.65 in Model K2-2 (Figure 3c). The occupancy ordering pattern of the [BO_3] groups within the partially occupied Hex-channels in Model K2-1 is in-phase and the occupancy ordering in Model K2-1 is out-of-phase. As a contrast, the occupancy ordering of ordered channel-[BO_3] in Model K2-2 is out-of-phase and the occupancy ordering of partially ordered channel-[BO_3] in Model K2-2 is in-phase. The B-O bond lengths of the framework [BO_3] and channel [BO_3] units are 1.35–1.40 Å and 1.35–1.37 Å respectively in Model K2-1 and 1.36–1.41 Å and 1.34–1.35 Å respectively in Model K2-2. Both models have chemically reasonable bond lengths.

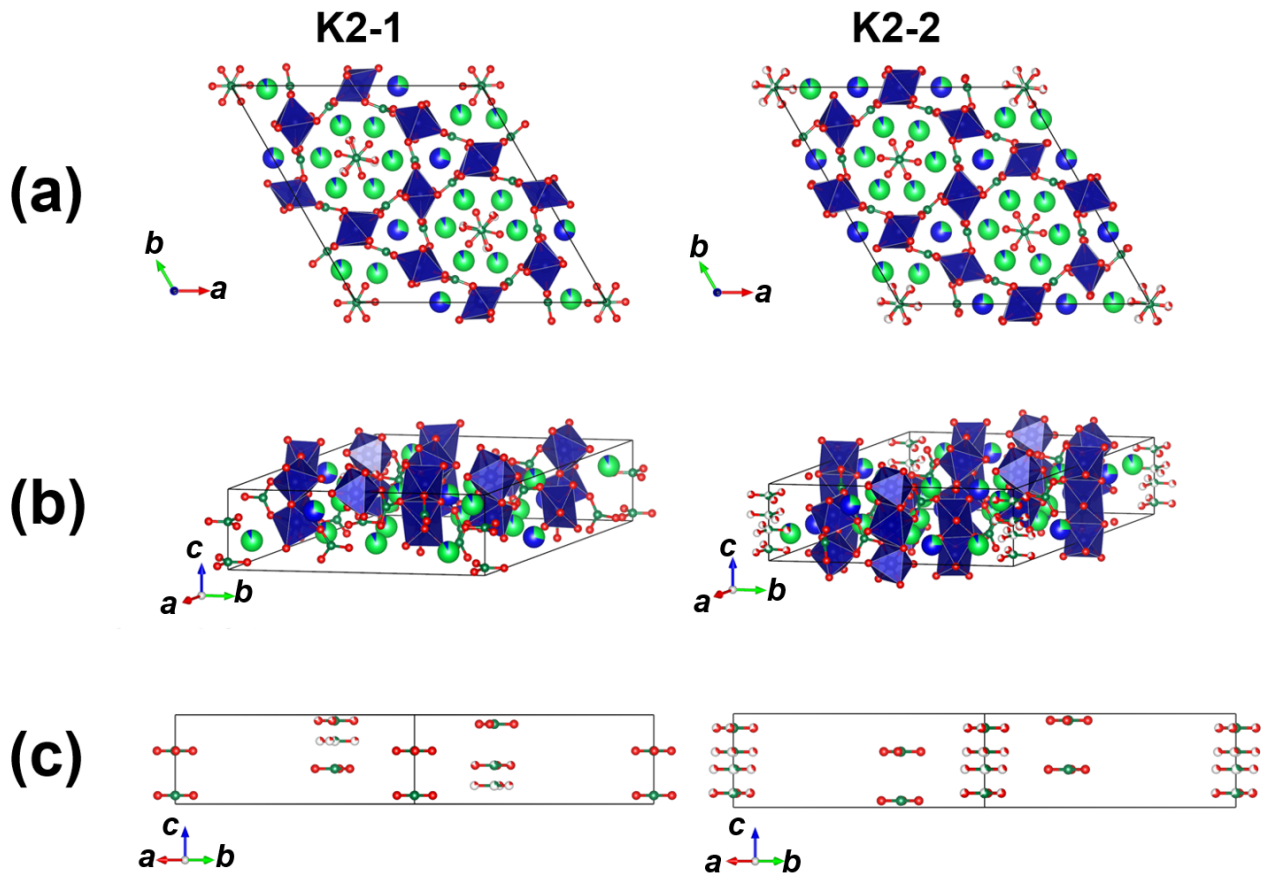

Figure 3. Crystal structure of two $YCa_3(CrO)_3(BO_3)_4$ models. (a) top view; (b) side view; (c) side view perpendicular to the long a-b diagonal with only the channel [BO_3] units shown. Red = O, small green = B, blue = Y, big green = Ca. [CrO_6] octahedra are drawn. The partial colouring of balls indicates mixed occupancy.

Table 1. Structural parameters of $YCa_3(CrO)_3(BO_3)_4$ in the K2-1 model. Space group $P6_3$ (#173), a = b = 18.1258(2) Å, c = 5.85954(8) Å. The atomic displacement parameters of the chemically equivalent ions were constrained to be equal to reduce the number of variables. (B_{eq} values for the B atoms were fixed to be identical to those of O atoms).

	Wyckoff site	*x*	*y*	*z*	Occupancy	B_{eq} (Å^2)
Ca1/Y1	6*c*	0.3332(12)	0.3351(11)	0.25	0.299(8)/0.701(8)	0.23(6)
Ca2/Y2	6*c*	-0.0155(12)	0.8495(13)	0.270(5)	0.900(3)/0.100(3)	0.23(6)
Ca3/Y3	6*c*	0.3328(10)	0.5252(11)	0.248(6)	0.900(3)/0.100(3)	0.23(6)
Ca4/Y4	6*c*	0.6548(13)	0.1833(14)	0.237(6)	0.900(3)/0.100(3)	0.23(6)
Cr1	6*c*	0.1710(15)	0.8324(15)	-0.015(5)	1	0.23(6)
Cr2	6*c*	0.5049(14)	0.4993(13)	-0.019(4)	1	0.23(6)
Cr3	6*c*	0.8396(15)	0.1682(14)	-0.007(5)	1	0.23(6)
B1	6*c*	0.7641(18)	0.7658(17)	0.234(7)	1	0.78(9)
B2	6*c*	0.0954(15)	0.4390(16)	0.257(9)	1	0.78(9)
B3	6*c*	0.4467(14)	0.1061(16)	0.252(8)	1	0.78(9)
B4	2*a*	0	0	0.096(6)	1	0.78(9)
B5	2*b*	1/3	2/3	0.206(13)	0.20(2)	0.78(9)
B6	2*b*	1/3	2/3	0.896(6)	1	0.78(9)
B7	2*b*	1/3	2/3	0.434(6)	0.80(2)	0.78(9)
O1	6*c*	0.1950(17)	0.2849(15)	0.263(7)	1	0.78(9)
O2	6*c*	0.5145(14)	0.9534(14)	0.275(6)	1	0.78(9)
O3	6*c*	0.8589(16)	0.6112(14)	0.244(7)	1	0.78(9)
O4	6*c*	0.8223(12)	0.7370(12)	0.220(7)	1	0.78(9)
O5	6*c*	0.1630(13)	0.4227(11)	0.277(8)	1	0.78(9)
O6	6*c*	0.5033(11)	0.0757(15)	0.251(8)	1	0.78(9)

O7	6*c*	0.7412(14)	0.7839(15)	0.032(7)	1	0.78(9)
O8	6*c*	0.4172(13)	0.1271(12)	0.063(7)	1	0.78(9)
O9	6*c*	0.0801(15)	0.4512(15)	0.033(7)	1	0.78(9)
O10	6*c*	0.7401(14)	0.7814(14)	0.447(8)	1	0.78(9)
O11	6*c*	0.0721(14)	0.4458(16)	0.476(7)	1	0.78(9)
O12	6*c*	0.4058(14)	0.1075(16)	0.448(8)	1	0.78(9)
O13	6*c*	0.0761(12)	0.0026(11)	0.096(6)	1	0.78(9)
O14	6*c*	0.395(5)	0.645(5)	0.206(13)	0.20(2)	0.78(9)
O15	6*c*	0.2702(15)	0.6858(14)	0.896(6)	1	0.78(9)
O16	6*c*	0.3446(18)	0.7468(17)	0.434(6)	0.80(2)	0.78(9)

Table 2. Structural parameters of $YCa_3(CrO)_3(BO_3)_4$ in the K2-2 model. Space group P-3 (#147), a = b = 18.12568(18) Å, c = 5.85949(7) Å. The atomic displacement parameters of the chemically equivalent ions were constrained to be equal to reduce the number of variables. (B_{eq} values for the B atoms were fixed to be identical to those of O atoms).

	Wyckoff site	*x*	*y*	*z*	Occupancy	B_{eq} (Å^2)
Ca1/Y1	6*g*	0.333(2)	0.333(2)	0.252(10)	0.266(7)/0.734(7)	0.14(6)
Ca2/Y2	6*g*	-0.008(2)	0.852(2)	0.260(9)	0.911(2)/0.089(2)	0.14(6)
Ca3/Y3	6*g*	0.321(2)	0.5219(16)	0.230(7)	0.911(2)/0.089(2)	0.14(6)
Ca4/Y4	6*g*	0.656(2)	0.184(2)	0.256(7)	0.911(2)/0.089(2)	0.14(6)
Cr1	6*g*	0.1690(18)	0.8353(17)	-0.013(3)	1	0.14(6)
Cr2	3*e*	0.5	0	0	1	0.14(6)
Cr3	6*g*	0.334(3)	0.1707(18)	0.491(3)	1	0.14(6)
Cr4	3*f*	0.5	0	0.5	1	0.14(6)
B1	6*g*	0.771(3)	0.770(3)	0.253(14)	1	0.78(9)
B2	6*g*	0.104(3)	0.437(3)	0.260(14)	1	0.78(9)
B3	6*g*	0.435(3)	0.106(3)	0.242(13)	1	0.78(9)
B4	2*c*	0	0	0.152(4)	0.65(4)	0.78(9)
B5	2*d*	1/3	2/3	0.929(7)	1	0.78(9)
B6	2*c*	0	0	0.592(17)	0.35(4)	0.78(9)
B7	2*d*	1/3	2/3	0.405(4)	1	0.78(9)
O1	6*g*	0.189(3)	0.290(2)	0.273(9)	1	0.78(9)
O2	6*g*	0.528(2)	0.945(2)	0.242(10)	1	0.78(9)
O3	6*g*	0.854(3)	0.617(3)	0.241(9)	1	0.78(9)
O4	6*g*	0.833(3)	0.744(3)	0.257(8)	1	0.78(9)
O5	6*g*	0.166(3)	0.411(3)	0.267(9)	1	0.78(9)

O6	6*g*	0.497(2)	0.082(3)	0.214(8)	1	0.78(9)
O7	6*g*	0.742(4)	0.785(4)	0.453(12)	1	0.78(9)
O8	6*g*	0.413(4)	0.119(4)	0.457(11)	1	0.78(9)
O9	6*g*	0.072(4)	0.446(4)	0.463(10)	1	0.78(9)
O10	6*g*	0.743(4)	0.780(4)	0.046(10)	1	0.78(9)
O11	6*g*	0.080(4)	0.454(4)	0.057(12)	1	0.78(9)
O12	6*g*	0.406(4)	0.114(4)	0.030(11)	1	0.78(9)
O13	6*g*	0.067(2)	-0.013(3)	0.152(4)	0.65(4)	0.78(9)
O14	6*g*	0.327(3)	0.589(3)	0.929(7)	1	0.78(9)
O15	6*g*	0.078(7)	0.071(8)	0.592(17)	0.35(4)	0.78(9)
O16	6*g*	0.254(3)	0.599(3)	0.405(4)	1	0.78(9)

Resistivity of $YCa_3(CrO)_3(BO_3)_4$. The temperature dependence of the resistivity was studied using impedance spectroscopy, a typical *Z*'−*Z*" impedance plot for $YCa_3(CrO)_3(BO_3)_4$ is given in Figure S2. The permittivity of these demonstrates the resistance is dominated by grain boundaries. The resistivity was estimated from the equivalent circuit fitting of the impedance data at different temperatures using a parallel Resistor (R) and constant phase element (CPE). At 24 °C, the sample resistivity ϱ is 10^8 Ωcm and the resistivity decreases as the temperature increases, indicative of an insulator (semiconductor). The activation energy for charge carrier migration in $YCa_3(CrO)_3(BO_3)_4$ was estimated to be 0.57(1) eV by an Arrhenius plot of the bulk conductivity (σ), Figure 4.

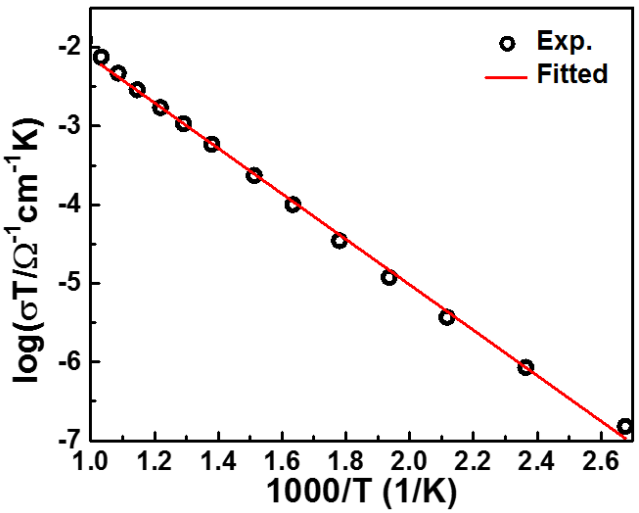

Figure 4. Arrhenius plots of $YCa_3(CrO)_3(BO_3)_4$ pellet.

Band gap of $YCa_3(CrO)_3(BO_3)_4$. The diffuse reflectance/absorbance spectrum of $YCa_3(CrO)_3(BO_3)_4$ is shown in Figure S3. For a solid material, the absorption coefficient α and the optical band gap E_g have the form[23]

$$\alpha h\nu = C\left(h\nu - E_g\right)^n \quad (1)$$

where h is Planck's constant, ν is frequency of vibration, and C is a constant. The power n differs with the band gap type, e.g., n = ½ for a direct allowed band gap and n = 2 for an indirect band gap.[24] The absorbance spectrum of $YCa_3(CrO)_3(BO_3)_4$ can be described by a direct band gap scheme. The $(h\nu\alpha)^2 - h\nu$ curve of $YCa_3(CrO)_3(BO_3)_4$ is plotted in Figure 5, from which the band gap E_g is estimated to be 1.65 eV. There is evidence for a second transition at 1.78 eV which may be due to a further splitting of the t_{2g} orbital band into two sub-bands by local distortion of $[CrO_6]$ octahedra from ideal geometry (the site symmetry of Cr^{3+} in K2-1 and K2-2 models is 1 and 1/i respectively.).

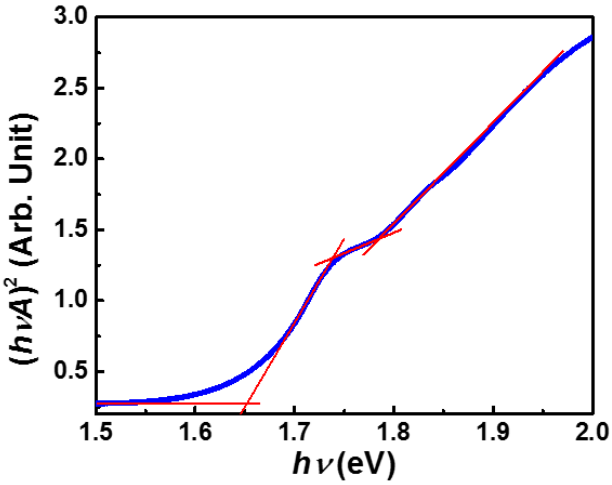

Figure 5. Absorption spectrum of $YCa_3(CrO)_3(BO_3)_4$ according to the direct band gap relation. The band gap E_g = 1.65 eV and another transition at ~1.78 eV can be seen.

Magnetic properties of $YCa_3(CrO)_3(BO_3)_4$. The temperature dependence of the molar magnetic susceptibility, χ_m, of $YCa_3(CrO)_3(BO_3)_4$ is shown in Figure 6. A comparison of the zero field-cooled (ZFC) and field-cooled (FC) susceptibility curves is shown in the inset Figure 6a. An upturn in the susceptibility is seen below ~20 K, but no Néel transition or divergence of ZFC-FC magnetic susceptibilities is observed down to 2 K, indicating that the sample does not undergo long-range antiferromagnetic (AFM) ordering or spin freezing, down to at least that temperature. The high-temperature magnetic susceptibility obeys the Curie-Weiss (CW) law $\chi_m = C/(T - \Theta)$, where Θ is the characteristic Weiss temperature and C is the Curie constant (inset Figure 6b). Least-squares fitting gives μ_{eff} = 3.92(1) μ_B/Cr^{3+}, which agrees well with the theoretical magnetic moment (3.88 μ_B) of the Cr^{3+} (d^3, S = 3/2) ion, and Θ = -120 K, suggesting relatively strong AFM exchange among the Cr^{3+} ions, despite the failure to observe a long-range magnetic ordering down to at 2 K.

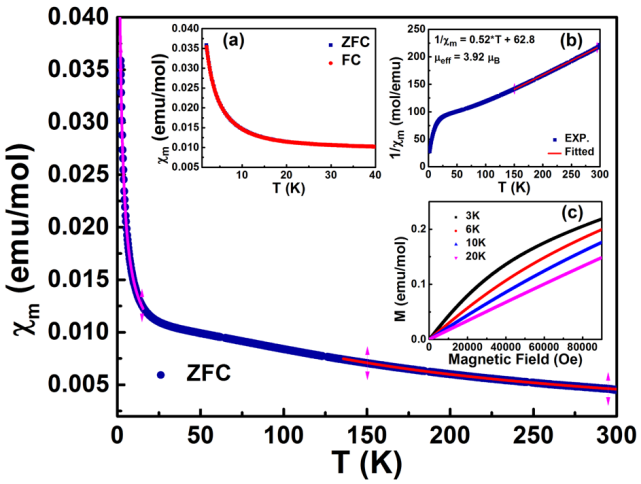

Figure 6. Temperature dependence of molar magnetic susceptibility (χ_m, per Cr^{3+}) of $YCa_3(CrO)_3(BO_3)_4$ collected in a coercive field of 1000 Oe. The red line is a Curie-Weiss fit to the high-temperature paramagnetic region, while the pink line is a fit to a Curie tail from ~4.4% paramagnetic spins per Cr^{3+}. The insets are (a) zero field-cooled (ZFC) and field-cooled (FC) temperature dependent molar magnetic susceptibility; (b) ZFC inverse susceptibility curve with a linear Curie-Weiss fit above 150 K; (c) field dependent molar magnetization M at 3, 6, 10 and 20 K.

The upturn in the magnetic susceptibility at very low temperatures (below ~20 K) is quite common in kagomé-lattice materials. This so-called "Curie tail" effect is typically interpreted as a contribution of para/ferromagnetic impurities[25] or paramagnetic defects in the material itself[26-28]. In order to differentiate between these possibilities, we collected further susceptibility data at higher coercive fields of 0.5, 1 and 5 T (presented in the SI). In the case of ferromagnetic impurities, higher coercive fields should suppress their contributions; this did not happen, therefore the tail is paramagnetic in origin. A Curie fit to the low-temperature region at 0.1 T yielded an estimate of 4.4% paramagnetic defects/impurities per Cr^{3+}.

The magnetic properties of $YCa_3(CrO)_3(BO_3)_4$ are most usefully discussed with respect to those of its neighbouring transition metal analogues. $YCa_3(MnO)_3(BO_3)_4$ (high-spin Mn^{3+}, d^4, $S = 2$) has a Weiss constant $\Theta = 27.2$ K, and undergoes a long-range FM ordering transition at $T_N = 7.5$ K[11]. The positive Weiss constant is due to FM interactions along the edge-sharing MnO_6 octahedral chains, and is consistent with the Goodenough-Kanamori rules for 90° superexchange between filled and empty e_g orbitals, while within the planes the Mn cations adopt the standard "$q = 0$" AFM ordered kagomé state below T_N.

$YCa_3(VO)_3(BO_3)_4$ (V^{3+}, d^2, $S = 1$) has a Weiss constant $\Theta = -453$ K and shows no sign of long-range magnetic order down to at least 3 K[12], making it one of the most strongly frustrated GFM kagomé systems known ($|\Theta/T_N| > 150$). The negative Weiss constant in this case is ascribed to dominant AFM interactions along the edge-sharing VO_6 octahedral chains, consistent with the Goodenough-Kanamori rules for 90 ° superexchange among empty t_{2g} orbitals. These AFM interactions along the chains are thought to be reinforced by direct overlap of the V^{3+} t_{2g} orbitals through the shared octahedral edges. Below ~150 K, an upturn in magnetic susceptibility was observed [12] which suggests the onset of FM V–O–O–V interactions in the kagomé plane. Temperature-dependent heat capacity data showed a weak peak at 2.8 K which could be evidence for short-range magnetic order, however this was not supported by AC or DC magnetic susceptibility measurements.

$YCa_3(CrO)_3(BO_3)_4$ (Cr^{3+}, d^3, $S = 3/2$) would be expected to behave more similarly to the V^{3+} case, since both have an empty e_g manifold in common, than the Mn^{3+} case; and indeed, the negative Weiss constant $\Theta = -120$ K can be understood in terms of the same Goodenough-Kanamori superexchange along the edge-sharing CrO_6 octahedral chains reinforced by direct exchange between Cr^{3+} t_{2g} orbitals. The development of a slight curvature in the M-H curves below ~20 K

(inset Figure 6c), may also be indicative of FM Cr–O–O–Cr super-superexchange interactions within the kagomé plane, although we note that this onset temperature is significantly lower than found in the analogous vanadate (~150 K).

Figure 7 shows the temperature-dependent heat capacity of $YCa_3(CrO)_3(BO_3)_4$ down to 1.9 K. A small and weak deviation from monotonic behaviour is apparent around 20 K, which is more clearly visible in the inset to Figure 7 after subtracting an empirical lattice contribution (3rd-order polynomial fit above 40 K). The deviation is much broader and less well-defined than the lambda-like anomalies typical of phase transitions, consistent with the absence long-range antiferromagnetic (AFM) ordering or spin freezing in our magnetic data. Noting that the maximum deviation coincides with the upturn in magnetic susceptibility and the development of curvature in the M-H curves below ~20 K, it is reasonable to conclude that this indicates the onset of local FM interactions within the kagomé plane.

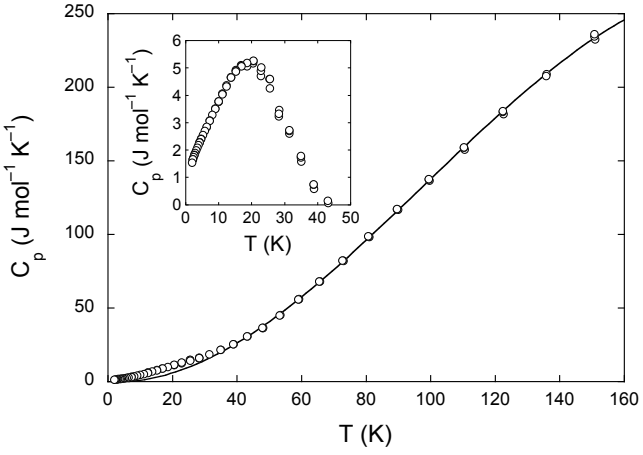

Figure 7. Temperature dependence of the heat capacity of $YCa_3(CrO)_3(BO_3)_4$. The line is an empirical fit to the lattice contribution above 40 K. The inset shows the difference between this fit and the experimental data at low temperatures.

CONCLUSIONS

$YCa_3(CrO)_3(BO_3)_4$ adopts a gaudefroyite-type structure featuring Cr^{3+} ions ($3d^3$, $S = 3/2$) on an undistorted kagomé lattice. High-purity samples were obtained by using a flux agent during synthesis, which significantly accelerates the reaction time and allows the use of lower temperatures, avoiding the problems associated with vitrifying borates. $YCa_3(CrO)_3(BO_3)_4$ has a [(2,1,0)(-1,1,0)(0,0,1)] supercell relative to $YCa_3(MnO)_3(BO_3)_4$, with a higher degree of Ca/Y ordering but a more ambiguous [BO_3] ordering pattern than $YCa_3(VO)_3(BO_3)_4$ with the same supercell. Rietveld fits of comparable quality to XRD and ND data were obtained with two alternative [BO_3] ordering models: K2-1 in the space group $P6_3$ (#173); and K2-2 [corresponding to the published model for $YCa_3(VO)_3(BO_3)_4$] in the space group $P\bar{3}$ (#147). However, this subtle crystallographic distinction between these [BO_3] ordering models has no obvious implications for the interpretation of the electronic and magnetic properties of $YCa_3(CrO)_3(BO_3)_4$, as discussed in the paper.

$YCa_3(CrO)_3(BO_3)_4$ is an insulator with the major band gap at $E_g = 1.65$eV and a second transition at 1.78 eV. It has strong AFM exchange (Weiss constant of $\Theta = -120$ K) along edge-sharing $Cr^{3+}O_6$ octahedral chains, due to a combination of Cr-O-Cr superexchange and Cr-Cr direct exchange. Cr–O–O–Cr super-superexchange interactions perpendicular to these chains appears to be FM but is much weaker, with no sign of long-range magnetic ordering or spin freezing down to at least 2 K. The fact that Cr^{3+} sites in these planes lie on an undistorted kagomé lattice raises an obvious question concerning the role of geometric magnetic frustration in $YCa_3(CrO)_3(BO_3)_4$, the answer to which depends on the sign of the in-plane super-superexchange which remains unresolved down to the lowest temperatures that we have been able to access. This merits further investigation in future ultra-low temperature experiments.

Supporting Information. Figure S1: Rietveld refinement profiles of $YCa_3(CrO)_3(BO_3)_4$ a using three models Model I, Model K2-1 and Model K2-2. Figure S2: *Z*'−*Z*" impedance plot for $YCa_3(CrO)_3(BO_3)_4$ at 100, 300, 500, and 700°C. Figure S3: Absorption spectrum of $YCa_3(CrO)_3(BO_3)_4$. Figure S4: Temperature dependence of molar magnetic susceptibility (χ_m, per Cr^{3+}) of $YCa_3(CrO)_3(BO_3)_4$ at different fields. Figure S5: Curie-Weiss fit of ZFC $YCa_3(CrO)_3(BO_3)_4$ χ_m -*T* curves over two different temperature ranges, 150–300 K and <15 K. K2_1_P63.cif, K2_2_P-3.cif and Model_I.cif: refined CIF files, as discussed in the paper.

AUTHOR INFORMATION

*Corresponding Author: Chris D. Ling, email: chris.ling@sydney.edu.au

FUNDING SOURCE

We acknowledge the Australian Research Council (Grant No. DP150102863) for support of this work.

REFERENCES

(1) Balents, L. *Nature* **2010**, *464*, 199-208.
(2) Capriotti, L.; Becca, F.; Parola, A.; Sorella, S. *Phys. Rev. Lett.* **2001**, *87*, 097201.
(3) Ramirez, A. P. *Annu. Rev. Mater. Sci.* **1994**, *24*, 453-480.
(4) Moessner, R.; Ramirez, A. R. *Phys. Today* **2006**, *59*, 24-29.
(5) Gardner, J. S.; Dunsiger, S. R.; Gaulin, B. D.; Gingras, M. J. P.; Greedan, J. E.; Kiefl, R. F.; Lumsden, M. D.; MacFarlane, W. A.; Raju, N. P.; Sonier, J. E.; Swainson, I.; Tun, Z. *Phys. Rev. Lett.* **1999**, *82*, 1012-1015.
(6) Harris, M. J.; Bramwell, S. T.; Holdsworth, P. C. W.; Champion, J. D. M. *Phys. Rev. Lett.* **1998**, *81*, 4496-4499.
(7) Jouravsky, F.; Permingeat, G. *Bulletin de la Société française de minéralogie et de cristallographie* **1964**, *87*, 216-219.
(8) Granger, M. M.; Protas, J. *Comptes Rendus Hebdomadaires Des Seances De L Academie Des Sciences* **1965**, *260*, 4553-4555.
(9) Li, R. K.; Greaves, C. *Phys. Rev. B* **2004**, *70*, 132411.
(10) Yu, Y.; Wu, Q. S.; Li, R. K. *J. Solid State Chem.* **2006**, *179*, 429-432.
(11) Li, R. K.; Greaves, C. *Phys. Rev. B* **2003**, *68*, 172403.
(12) Miiller, W.; Christensen, M.; Khan, A.; Sharma, N.; Macquart, R. B.; Avdeev, M.; McIntyre, G. J.; Piltz, R. O.; Ling, C. D. *Chem. Mater.* **2011**, *23*, 1315-1322.
(13) Inami, T.; Morimoto, T.; Nishiyama, M.; Maegawa, S.; Oka, Y.; Okumura, H. *Phys. Rev. B* **2001**, *64*, 054421.
(14) Nishiyama, M.; Morimoto, T.; Maegawa, S.; Inami, T.; Oka, Y. *Can. J. Phys.* **2001**, *79*, 1511-1516.
(15) Martinez, B.; Sandiumenge, F.; Rouco, A.; Labarta, A.; Rodriguezcarvajal, J.; Tovar, M.; Causa, M. T.; Gali, S.; Obradors, X. *Phys. Rev. B* **1992**, *46*, 10786-10792.
(16) Liss, K.-D.; Hunter, B.; Hagen, M.; Noakes, T.; Kennedy, S. *Physica B: Condensed Matter* **2006**, *385–386, Part 2*, 1010-1012.
(17) Coelho, A. A.; Evans, J. S. O.; Evans, I. R.; Kern, A.; Parsons, S. *Powder Diffr.* **2011**, *26*, S22-S25.
(18) Evans, J. S. O. In *Extending the Reach of Powder Diffraction Modelling by User Defined Macros*; Scardi, P., Dinnebier, R. E., Eds. 2010; Vol. 651, p 1-9.
(19) Campbell, B. J.; Stokes, H. T.; Tanner, D. E.; Hatch, D. M. *J. Appl. Crystallogr.* **2006**, *39*, 607-614.
(20) Poole, R. T.; Jenkin, J. G.; Liesegang, J.; Leckey, R. C. G. *Phys. Rev. B* **1975**, *11*, 5179-5189.
(21) Sears, V. F. In *International tables for crystallography*; 3 ed.; Prince, E., Ed. 2004; Vol. C, p 444-454.
(22) Halasyamani, P. S.; Poeppelmeier, K. R. *Chem. Mater.* **1998**, *10*, 2753-2769.
(23) Al-Ani, S. K. J. *Int. J. Electron.* **1993**, *75*, 1153-1163.
(24) Miller, A. In *HANDBOOK OF OPTICS, Volume I: Fundamentals , Techniques , and Design*; Bass, M., Stryland, E. W. V., Williams, D. R., Wolfe, W. L., Eds.; McGRAW-HILL , INC . New York, 1995, p 9.1-9.33.
(25) Donakowski, M. D.; Lu, H.; Gautier, R.; Saha, R.; Sundaresan, A.; Poeppelmeier, K. R. *Z. Anorg. Allg. Chem.* **2014**, *640*, 1109-1114.
(26) Limot, L.; Mendels, P.; Collin, G.; Mondelli, C.; Ouladdiaf, B.; Mutka, H.; Blanchard, N.; Mekata, M. *Phys. Rev. B* **2002**, *65*, 144447.

(27) Bert, F.; Bono, D.; Mendels, P.; Trombe, J. C.; Millet, P.; Amato, A.; Baines, C.; Hillier, A. *J. Phys.: Condens. Matter* **2004**, *16*, S829-S834.
(28) Okamoto, Y.; Yoshida, H.; Hiroi, Z. *J. Phys. Soc. Jpn.* **2009**, *78*, 033701.

For Table of Contents Only

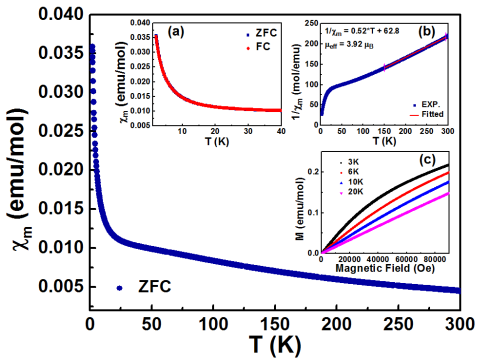

$YCa_3(CrO)_3(BO_3)_4$ with Cr^{3+} (S =3/2) sitting on kagomé lattice is strongly magnetic frustrated.